acta physica slovaca vol. 55 No. 2, 211 – 227 **April 2005**

A DESIGN OF A WAVELENGTH-HOPPING TIME-SPREADING INCOHERENT OPTICAL CODE DIVISION MULTIPLE ACCESS SYSTEM

I. Glesk[1,a,b], **V. Baby**[b], **C. S. Brès**[b], **L. Xu**[b], **P. R. Prucnal**[b], **W. C. Kwong**[c]
[a] *Department of Experimental Physics, Comenius University, 842 48 Bratislava, Slovakia*
[b] *Department of Electrical Engineering, Princeton University, Princeton, NJ 08540, USA*
[c] *Department of Engineering, Hofstra University, Hempstead, NY 11549, USA*

Received 5 October 2004, accepted 20 December 2004

We present the architecture and code design for a highly scalable, 2.5 Gb/s per user optical code division multiple access (OCDMA) system. The system is scalable to 100 potential and more than 10 simultaneous users, each with a bit error rate (BER) of less than 10^{-9}. The system architecture uses a fast wavelength-hopping, time-spreading codes. Unlike frequency and phase sensitive coherent OCDMA systems, this architecture utilizes standard on-off keyed optical pulses allocated in the time and wavelength dimensions. This incoherent OCDMA approach is compatible with existing WDM optical networks and utilizes off the shelf components. We discuss the novel optical subsystem designs for encoders and decoders that enable the realization of a highly scalable incoherent OCDMA system with rapid reconfigurability. A detailed analysis of the scalability of the two dimensional code is presented and select network deployment architectures for OCDMA are discussed.

PACS: 42.55.Wd, 42.81.Wg

1 Introduction

To deliver multimedia and bursty data content to a growing broadband user population, intense research and development have focused on the techniques for providing bandwidth efficient multiple access formats and protocols. Common techniques for accessing bandwidth in a multi-user environment on wireline networks have relied on wavelength-division multiple access (WDMA) and time-division multiple access (TDMA). Whereas both of these schemes have been utilized individually as well as concurrently in present-day optical communication systems, code-division multiple access (CDMA) scheme has so far been used more in RF wireless communication systems. In TDMA and WDMA, multiple-user access to shared bandwidth is allowed by assigning a time slot within an aggregated frame and by assigning a wavelength within a band of wavelengths respectively. These systems require strict enforcement of the synchronization of the users in the time domain or non-overlapping assignment of the wavelengths in the spectral domain. However, by allocating unique codes that are created by combining various parameters such as time slots,

[1]E-mail address: glesk@princeton.edu

frequency, polarization, and phase, CDMA systems enable asynchronous access to the entire bandwidth by different users of the communications channel. In addition, CDMA offers other advantages such as simplified network control, increased physical layer privacy and on-demand bandwidth sharing and bandwidth management. By extending these concepts into the optical domain, OCDMA promises to extend the flexibility and advantages of CDMA systems into the vast bandwidth provided by fiber-optics. These advantages make OCDMA a promising technology for future multiple-access networks. Many of the barriers to implementing OCDMA are perceived rather than fundamental limits of the available technology when taken in the context of a multi-user optical access network environment [1]. By leveraging recent advances in photonic components, WDM systems, and optical TDM systems, new architectures based on OCDMA are becoming more practical for future deployment.

In this paper, we present an approach to OCDMA that enables large scale, high speed multi-user access to shared optical bandwidth on a broadcast and select network architecture. Three critical areas in research on this system are being investigated: (i) advanced photonic encoding and decoding hardware and components; (ii) coding algorithms and techniques; and (iii) network architecture, scalability assessment, and applications. These three research areas span the technology needed to implement an advanced OCDMA system [2]. The theoretical foundation and technology are outlined in this paper and demonstrate the feasibility of developing an OCDMA system with 2.5 Gb/s per user and (BER) $< 10^{-9}$. Our system analysis indicates that the network will demonstrate scalability of more than 10 simultaneous users from a potential pool of more than 100 possible codes. Our approach applies novel coding algorithms to allocate sequences to optical bandwidth simultaneously across both wavelengths and time slots. New classes of two-dimensional optical codes are investigated and analytical results for the performance of a multi-user asynchronous access system are presented. The system also leverages recent innovations in ultrafast optical components and subsystems, including ultrafast time slot tuners, all-optical demultiplexers, and multi-wavelength laser sources. Finally, various system architectures and approaches to practical deployment of OCDMA in the context of the existing optical network infrastructure are presented.

2 Technical Rationale

CDMA is rapidly becoming the foremost technology in RF wireless communications because of the significant advantages it offers, such as enhanced detection in the presence of multi-user interference (MAI), higher spectral efficiency and robustness to multipath interference. In today's RF wireless CDMA communication systems carrier frequencies are in the range of $\sim$1 GHz, the typical bit rate is 10-100 kb/s, the typical chip widths are on the order of a few hundred nanoseconds, the bits are divided into a few hundred or thousand chips, and 1-D codes are formed by populating a subset of these chips. Each user is assigned a unique code and all the users can asynchronously transmit. The receiver intended for a user has to decode the assigned user's information in the presence of interference from other users, called MAI noise. This makes code orthogonality a key factor in CDMA systems, where orthogonality connotes the property of a large autocorrelation in comparison to a small or zero cross-correlation function. Families of codes having a large number of orthogonal codes, allowing a large number of users, are possible in RF wireless CDMA on account of the large number of chips in a bit period and the possibility

of utilizing bipolar codes. Since the data rates per user in an RF wireless CDMA network are relatively modest, the codes scale to support a large number of users usually in a single geographic area - cell.

The key distinction between the RF and optical domain is the vast amount of bandwidth provided in an optical fiber useable to a large user population communicating at very high bit rates (soon exceeding 10 Gb/s per user) while geographically separated by up to thousands of kilometers. In comparison to RF CDMA, the shorter duration of optical bit period (because of high bit rates) can limit the number of temporal chips the bit can be divided into, thus reducing the cardinality (the number of possible codes) in OCDMA systems. The cardinality can be even further constrained in incoherent OCDMA systems due to the unipolarity of the codes. Considering these differences, the constraints imposed by existing technology, and the effects of fiber optic transmission over metro/regional distances, we have optimized the code selection for optical CDMA. Through the optimized codes and proper hardware selection many of the perceived limitations of OCDMA systems can be reduced or eliminated all together.

To support many simultaneous users, 1-D optical codes, such as various prime codes [3] and optical orthogonal codes (OOCs) [4,5] were originally designed with good correlation properties (i.e., thumbtack-shape autocorrelation and very low cross-correlation functions) to discriminate between the correct sequence and interfering noise. However, most optical codes with these properties are also sparse in binary ones. This means that a very long code length is required to obtain a good extinction ratio (i.e., the ratio of autocorrelation peak to the maximum cross-correlation value). On other hand, due to practical hardware realizations a reduction of the code length might be required which could result in a reduction of the cardinality of the system. One possible way how to prevent this penalty is to access a second coding dimension - wavelength, and use so-called 2-D wavelength-time codes [6,7]. These codes can be viewed as fast wavelength-hopping codes, in which wavelength-hops take place at every pulse of a code sequence. In this area of 2-D coding, several coding algorithms have been reported. For example, prime-hop codes were constructed by using prime sequences to control the wavelength-hopping patterns, but had a limited cardinality [7]. Yim et al. studied the use of computers to search for wavelength-time codes [8]. In [9], Kim et al. introduced 3D unipolar pseudo-orthogonal codes, utilizing space, wavelength, and time dimensions simultaneously.

In areas of network-level analyses, little work associated with OCDMA has been performed. Although code assignment techniques, contention protocols, and power-control algorithms have been investigated for use in OCDMA networking environments [10,11], more research in these areas is required to develop scalable and robust systems that can be deployed.

3 System Overview

3.1 System Architecture

We have demonstrated an incoherent OCDMA system based on a wavelength-hopping, time-spreading coding technique using rapidly reconfigurable coding devices and novel ultra fast all optical time gating technology. The functional subsystems of the architecture are shown in Fig. 1. In this system, the encoder simultaneously modulates the data onto multiple optical

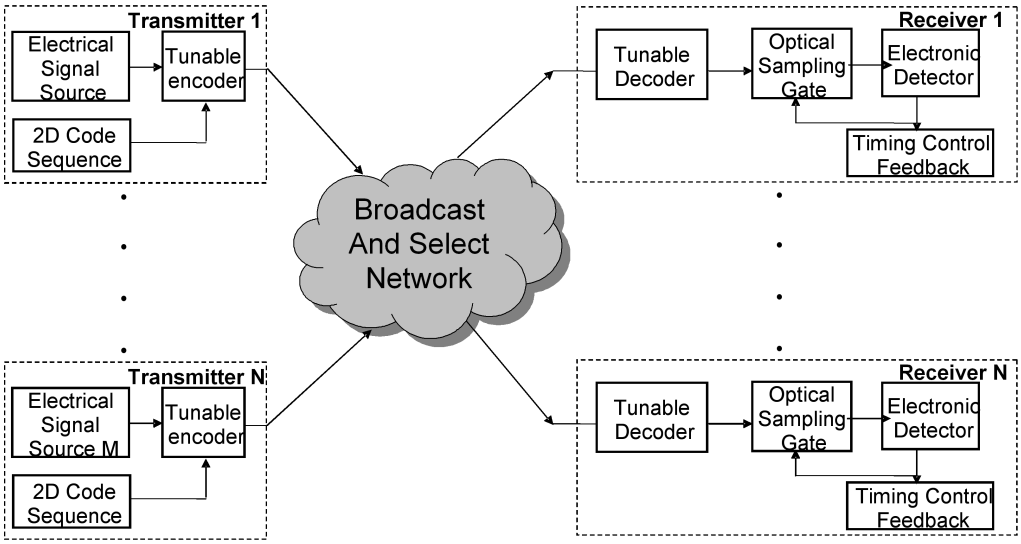

Fig. 1. Schematic of a broadcast and select OCDMA network.

pulses with different center wavelengths that are then allotted into different timeslots (chips) within a bit period. We use a carrier-hopping prime code [3], which is a class of wavelength-time codes. These codes allow every pulse in a two-dimensional code sequence to be encoded in a distinct wavelength and, thus, maintain zero autocorrelation sidelobes. Tunability at the encoder enables an individual user to dynamically select from the available codes on the network. The signals from multiple users are aggregated onto a broadcast network. At a receiver, a matched decoder recovers the data by performing an autocorrelation for a particular code assigned to that destination. To enhance the contrast of the autocorrelation peak, a second decoder with a complementary code sequence can also be used in conjunction with a balanced detector to further reduce the impact of multi-user interference. By using an ultrafast optical gate prior to photodetection, the autocorrelation peak can be separated from interference in other chips, to further improve the signal contrast at the detector. Timing control at the receiver aligns the optical gate with the desired autocorrelation peak. After photodetection and thresholding, the original transmitted data sequence is digitally recovered.

3.2 Component Design

3.2.1 Optical Transmitter Design

The schematic of an OCDMA transmitter/encoder design is shown in Fig. 2. A mode-locked laser is used to generate a broadband supercontinuum that is modulated with the transmitted digital binary sequence using on-off keying. A thin film filter (TFF) based WDM demultiplexer is used to slice the modulated supercontinuum into multiple wavelengths. Adjustable time delays separate and align each pulsed wavelength to form a time code. By leveraging ultrafast time delay selection techniques, the code can be rapidly changed to provide dynamic code allocation. The

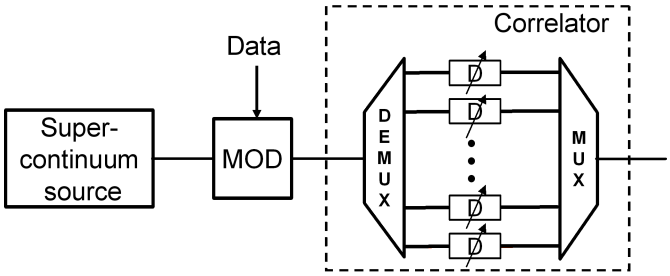

Fig. 2. Schematic of a tunable OCDMA encoder. MOD: modulator; D: tunable delay line.

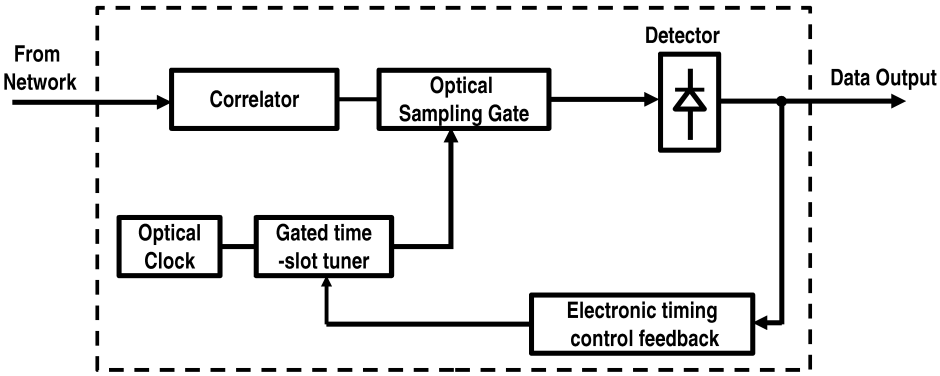

Fig. 3. Schematic of an OCDMA receiver.

individual wavelengths of the code are combined by a WDM multiplexer and transmitted into the network.

3.2.2 Optical Receiver Design

The basic function of the optical receiver is to distinguish the correct code sequence from the arriving wavelength-time OCDMA waveforms in the presence of MAI. The setup for our wavelength-time optical receiver is shown in Fig. 3. The correlator is setup similar to the encoder, except that the wavelength and the time-delay arrangements are in reverse order. This assures the formation of an autocorrelation peak at the correct receiver address, since the pulses in the code sequence would then be wavelength selected and time-delayed such that they overlap at the correlator output. Otherwise, the pulses cannot overlap, resulting in a low cross-correlation function.

By properly designing the code sequences, a significant reduction of MAI can be obtained. The electronic signals are then threshold detected and data bits are recovered. The asynchronous

nature of OCDMA systems require the detector to operate at the chip rate, which, to support more than 10 users at a data rate of at least 2.5 Gb/s approaches 100 GHz. The use of a detector directly at such a chip rate is not possible because of speed limitations on commercial photodetectors. However, by using a novel all-optical optical sampling gate the TOAD (see Section 5.2), ultra short gating functions in the time domain can be applied to the signal at the output of the correlator to reject most of the cross-correlation noise. A standard commercially available photodetector can then be used at the output of the sampling gate for signal recovery.

An electronic timing controller coupled to a gated time slot tuner is used to monitor the output of the balanced detector for tracking the arrivals of autocorrelation peaks and to adjust the optical sampling time delay during initial channel setup. While a receiver is idle, its decoder will continuously monitor the arriving waveforms to see if any transmitter is trying to establish a link with the receiver. This is done by (1) transmitters sending the code sequence corresponding to that of the receiver, and (2) the receiver continuously sweeping the optical gate control signal to discover the presence of autocorrelation peaks at different chip positions. Once the time location of the autocorrelation peak is confirmed, the tracking is finished and the tuner will be fixed. A hand-shaking protocol can be applied to facilitate this initial setup.

4 Codes

4.1 Carrier-Hopping Prime Code

The use of multiple wavelengths in OCDMA codes adds coding flexibility and, more importantly, improves code performance. In [7], Tancevski *et al.* introduced the prime-hop code, which had every pulse in each binary code sequence of the original prime code encoded at a distinct wavelength, resulting in a class of OOCs with zero autocorrelation side lobes and cross-correlation functions of at most one. For a given prime number p, p different wavelengths were used, and the prime-hop code had length, weight, and cardinality of p^2, p, and $p(p\text{-}1)$, respectively. By utilizing p wavelengths, the code provides a factor of p more code sequences than the original prime code. However, the cardinality is still limited and not flexible, as compared to the carrier-hopping prime code.

As in wireless communications, carrier hopping is usually referred to as frequency hopping (FH). Most of the FH codes studied are based on the Reed-Solomon codes [15]. For these codes, cardinality is usually controlled by the pre-selected maximum cross-correlation value and the number of hopping frequencies. Relaxing the maximum cross-correlation value to improve system cardinality is not feasible since it dramatically worsens the system outage probability. Thus, in practice, for such Reed-Solomon-based codes, cardinality can be improved only by increasing the number of frequencies, which will be prohibited in some band-limited applications. Therefore, it is advantageous to have codes, such as the carrier-hopping prime code, whose cardinality is a function of code length, not the pre-selected maximum cross-correlation value.

In this section, we construct the carrier-hopping prime code using a 2-D algebraic approach, where the code sequences are represented as $p_1p_2 \ldots p_k$ binary (0,1) matrices of length $p_1p_2 \ldots p_k$, weight w, and cardinality $p_1p_2 \ldots p_k$ for two given positive integers w and k and a set of prime numbers $\{p_1p_2 \ldots p_k\}$, where $p_k \geq p_{k-1} \geq \ldots \geq p_2 \geq p_1 \geq w$. Note that w is also the number of rows, related to the number of available carriers, and $p_1p_2 \ldots p_k$ is the number of columns, related to the length of the matrices. Because each matrix consists of one pulse per row and each

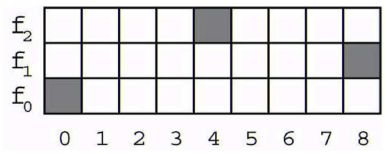

Fig. 4. The matrix representation of the carrier-hopping prime code sequence $f_0 00 \quad 0 f_2 0 \quad 00 f_1$. The black squares represent its ordered pairs. The horizontal and vertical numbers in the matrix represent the chip position and transmitting carrier index of the ordered pair respectively.

pulse in a matrix is assigned with a distinct carrier, the code has zero autocorrelation sidelobes (i.e., $\lambda_a = 0$) and cross-correlation function of at most one (i.e., $\lambda_c = 1$). With respect to the Reed-Solomon-based code, the carrier-hopping prime code has the advantage of improving the code cardinality without sacrificing the correlation property.

For ease of representation, every matrix can equivalently be written as a set of w ordered pairs (i.e., one ordered pair $(f_v,\ t_h)$ for every binary one), where f_v represents the transmitting carrier index and t_h shows the chip position of the binary one. For example, the carrier-hopping sequence $f_0 00 \quad 0 f_2 0 \quad 00 f_1$ can also be represented as a 3×9 matrix shown in Fig. 4, where the black squares represent the locations of the ordered pairs and their transmitting carriers depend on the rows in which they are located. The matrix can equivalently also be represented by a set of three ordered pairs [(0,0), (1,8), (2,4)].

4.1.1 Coding Algorithms

Because of the good correlation properties, the carrier-hopping prime code can be denoted as a class of $(w \times p_1 p_2 \ldots p_k, w, 0, 1)$ OOCs.

Definition: Let the $(L \times N, w, \lambda_a, \lambda_c)$ carrier-hopping prime code be a collection of binary (0,1) $L \times N$ matrices, each of Hamming weight w, with the maximum autocorrelation side lobe and cross-correlation function no more than λ_a and λ_c, respectively. In general, given two positive integers w and k and a set of prime numbers $\{p_1 p_2 ... p_k\}$, such that $p_k \geq p_{k-1} \geq ... \geq p_2 \geq p_1 \geq w$, matrices $x_{i1,i2...,ik}$, with the ordered pairs

$$\left\{ \begin{array}{l} \left[\begin{array}{l} (0,0), (1, i_1 + i_2 p_1 + ... + i_k p_1 p_2 ... p_{k-1}), \\ (2, 2 \otimes_{p1} i_1 + (2 \otimes_{p2} i_2) p_1 + ... + (2 \otimes_{pk} i_k) p_1 p_2 ... p_{k-1}), ..., \\ (w-1, (w-1) \otimes_{p1} i_1 + ((w-1) \otimes_{p2} i_2) p_1 + ... \\ + ((w-1) \otimes_{pk} i_k) p_1 p_2 ... p_{k-1}) \end{array} \right] : \\ i_1 = \{0, 1, ..., p_1 - 1\}, i_2 = \{0, 1, ..., p_2 - 1\}, ..., i_k = \{0, 1, ..., p_k - 1\} \end{array} \right\}$$

form the $(w \times p_1 p_2 ... p_k, w, 0, 1)$ carrier-hopping prime code with $p_1 p_2 ... p_k$ matrices of length $p_1 p_2 ... p_k$ and weight w, where "$\otimes_{pj}$" denotes a modulo-p_j multiplication for $j = \{1, 2, 3, ..., k\}$.

The original prime code used in [13] is a subset of carrier-hopping prime code with k = 1, $w = p_1$ and only one transmitting carrier. Similarly, the prime-hop code in [7] uses $k = 2$, $w = p_1 = p_2$ and is based on the choice of $k = 2$ minus $k = 1$. Therefore, it has $p_1 (p_1 - 1)$ matrices, p_1 less than the carrier-hopping prime code with the same code parameters.

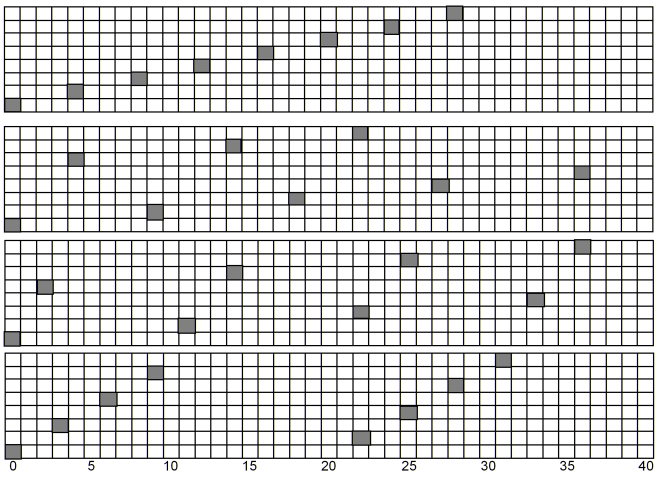

Fig. 5. Examples of the (8 × 41, 8, 0, 1) carrier-hopping prime code. The four matrices represent the code sequences x_4, x_9, x_{11}, and x_{22}, respectively.

Using $k = 1$, $p_1 = 41$, and $w = 8$ as an example, this carrier-hopping prime code has 41 matrices, x_{i1} (for $i_1 \in [0, 40]$), represented by the ordered pairs [(0,0), (1,i_1), (2,2$\otimes_{41} i_1$), (3,3$\otimes_{41} i_1$), ..., (7,7$\otimes_{41} i_1$)]. Figure 5 shows the matrices x_4, x_9, x_{11}, and x_{22}, respectively.

Table 1 shows the cardinality, length, weight, and the maximum cross-correlation value λ_c of the Reed-Solomon-based codes [15,16] and carrier-hopping prime codes, where the number of carriers is fixed to a prime number p (i.e., $w = p$). When cardinality is equal to p, both families give comparable performance. The Reed-Solomon-based codes, however, have to relax λ_c from one to two in order to have a cardinality of p^2. Instead, the improvement in cardinality can be done in the carrier-hopping prime code solely by increasing the code length to p^2 without sacrificing λ_c.

Tab. 1. Cardinality, length, weight, and maximum cross-correlation value λ_c of the Reed-Solomon-based codes and carrier-hopping prime code. The number of carriers is fixed to a prime number p.

	Reed-Solomon		Carrier-hopping Prime	
	$w = p$ [29]	$w = p$ [30]	$k = 1$, $w = p_1 = p$	$k = 2$, $w = p_1 = p_1 = p$
Cardinality	p	p^2	p	p^2
Length	$p-1$	$p-1$	p	p^2
Weight	$p-1$	$p-1$	p	p
λ_c	1	2	1	1

4.1.2 Correlation Properties

Definition: The $(L \times N, w, \lambda_a, \lambda_c)$ carrier-hopping prime code, C, is a collection of binary (0,1) $L \times N$ matrices, each of Hamming weight w, such that the following properties hold [7]:

a) *Autocorrelation:* For any matrix $x \in C$ and integer $\tau \in [1, N-1]$, the binary discrete two-dimensional autocorrelation sidelobe of x is no greater than a nonnegative integer λ_a, such that $\sum_{i=0}^{L-1} \sum_{j=0}^{N-1} x_{i,j} x_{i,j\oplus\tau} \leq \lambda_a$, where $x_{i,j} = \{0,1\}$ is an element of x at the ith row and j-th column and "$\oplus$" denotes a modulo-N addition [3].

b) *Cross-correlation:* For any two distinct matrices $x \in C$ and y $\in C$ and integer $\tau \in [1, N-1]$, the binary discrete two-dimensional cross-correlation function of x and y is no greater than a positive integer λ_c, such that $\sum_{i=0}^{L-1} \sum_{j=0}^{N-1} x_{i,j} y_{i,j\oplus\tau} \leq \lambda_c$, where $y_{i,j} = \{0,1\}$ is an element of y at the i-th row and j-th column [3].

4.1.3 Cardinality

In this section, the upper bound of the cardinality of the carrier-hopping prime code and its optimality are studied. Let $\Phi(L \times N, w, \lambda_a, \lambda_c)$ be the upper bound of the cardinality of the $(L \times N, w, \lambda_a, \lambda_c)$ carrier-hopping prime code, such that $\Phi(L \times N, w, \lambda_a, \lambda_c) \cong \max\{|C| : C$ is the $(L \times N, w, \lambda_a, \lambda_c)$ carrier-hopping prime code$\}$, where $L \times N$ is the size of each matrix, w is the code weight, λ_a is the maximum autocorrelation sidelobe, and λ_c is the maximum cross-correlation value.

To show that the carrier-hopping prime code is asymptotically optimal, the upper bound of the code cardinality is derived by multiplying the Johnson bound for the OOCs in [4,5] with L available carriers, and is given by

$$\Phi(L \times N, w, \lambda, \lambda) \leq \frac{L(LN-1)(LN-2)...(LN-\lambda)}{w(w-1)...(w-\lambda)}, \tag{1}$$

where the maximum autocorrelation sidelobe and cross-correlation values are assumed to be identical (i.e., $\lambda = \lambda_a = \lambda_c$).

Therefore, the upper bound in (1) for the carrier-hopping prime code with $L = w$, $N = p_1 p_2 \ldots p_k$, $\lambda_a = 0$, and $\lambda_c = 1$ can be modified to

$$\begin{aligned} \Phi(w \times p_1 p_2 ... p_k, w, 0, 1) &\leq (w \times p_1 p_2 ... p_k, w, 1, 1) \\ &\leq \frac{w(w p_1 p_2 ... p_k - 1)}{w(w-1)} \\ &= p_1 p_2 ... p_k + \frac{p_1 p_2 ... p_k - 1}{w-1} \end{aligned} \tag{2}$$

The ratio of the cardinality of the $(w \times p_1 p_2 ... p_k, w, 0, 1)$ carrier-hopping prime code (i.e., $p_1 p_2 ... p_k$) to (2) is found to be $1/[1 + 1/(w-1) - 1/(w p_1 p_2 ... p_k)]$. The ratio is nearly equal to one for a large w. The carrier-hopping prime code is, thus, asymptotically optimal.

4.1.4 Performance Analysis

To analyze the performance of a multiwavelength OCDMA system with the $(L \times N, w, 0, 1)$ carrier-hopping prime code, the probability q to line up (or hit) one of the pulses in a signature matrix, say x, with a pulse in another matrix, say y, is needed [17]. Because the carrier-hopping prime code has at most one pulse per row and column in each matrix, we have $q = \frac{w^2}{2LNx}$, where the factor 1/2 comes from the assumption of equiprobable 0–1 data-bit transmissions and x is equal to a chip width divided by the width of optical sampling window.

Let Th and K denote the decision threshold of the receiver and total number of simultaneous users in the system, respectively. The error probability of the wavelength-time OCDMA scheme with the carrier-hopping prime code and hard limiting is then given by

$$P_e = \frac{1}{2}\sum_{i=0}^{Th}(-1)^i \binom{w}{i} \left(1 - \frac{iq}{w}\right)^{K-1}, \tag{3}$$

where Th is usually set to the code weight w for optimal operation.

The probabilities of error P_e of the $(L \times N, L, 0, 1)$ carrier-hopping prime code versus the number of simultaneous users K is plotted in Fig. 6 for various values of L and N. In general, the error probability improves as the number of wavelengths (i.e., L) and/or the number of chips (i.e., N) increase. Because of the coding flexibility, the carrier-hopping prime code allows the adjustment of the number of wavelengths, the number of chips, or both, in order to achieve a predetermined BER performance at a given K.

5 Technology

5.1 Multi-wavelength Laser Source

To obtain narrow optical pulses at different wavelengths, the multi-wavelength laser source used is a mode-locked Erbium-doped fiber laser with a nonlinear fiber pulse compressor. Pulses as short as tens of femtoseconds with 10–40 GHz repetition rate can be generated.

The multi-wavelength source is based on the principle of supercontinuum generation, represented in Fig. 7. A high-powered short optical pulse is injected into a span of dispersion decreasing fiber (DDF). The high peak power of the laser generates additional spectral components through the nonlinearity in the DDF, whereas the dispersion profile of the fiber maintains the temporal pulse width through the length of the fiber [18]. At the output of the DDF, the supercontinuum pulse is spectrum-sliced through the use of a TFF based WDM demultiplexer. Over 20 nm of optical bandwidth was generated with an output optical pulse width of 1.6 ps. The use of supercontinuum generation technique to create the multi-wavelength optical pulses enables the use of one laser as opposed to separate lasers at each individual wavelength.

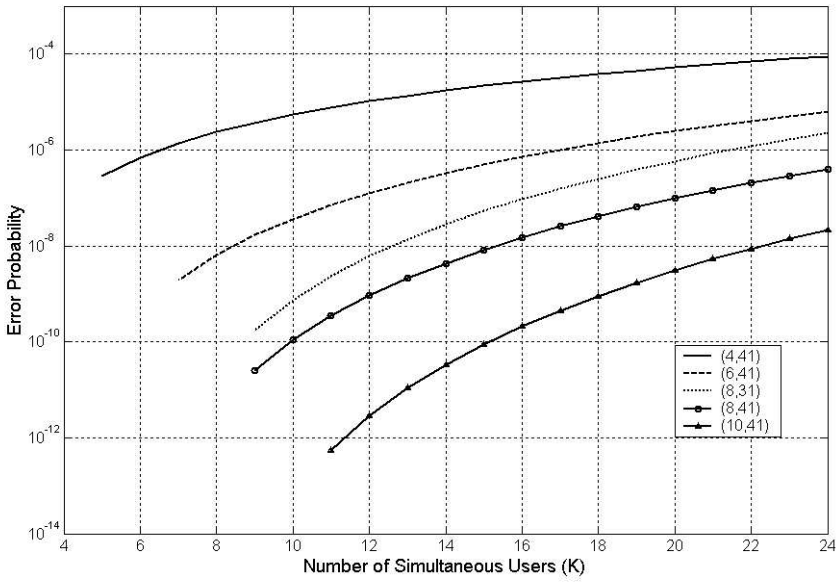

Fig. 6. Probability of error P_e of the (N, L) carrier-hopping prime code versus the number of simultaneous users K, including optical sampling, hard limiting and chip asynchronization, where L is number of wavelength and N is number of timeslots.

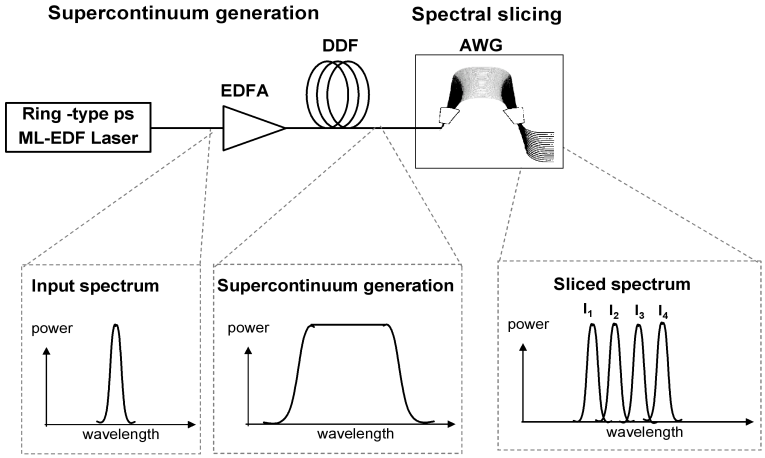

Fig. 7. Multi-wavelength source: Supercontinuum generation and spectrum-slicing of the broad spectrum. The inset shows the spectrum at different positions.

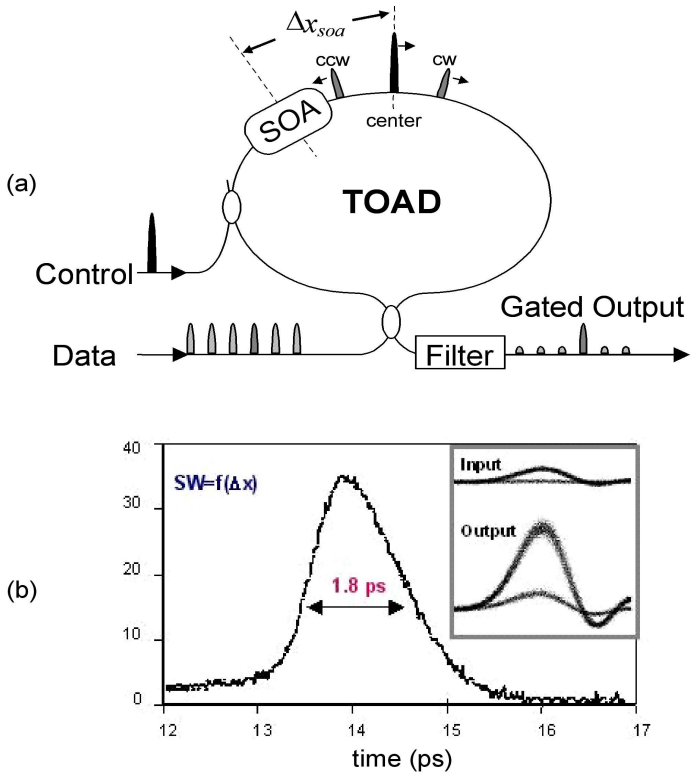

Fig. 8. (a) Schematic of the TOAD; (b) Normalized intensity at the output of the TOAD. Inset: Eye-diagrams at the input and output ports of the TOAD. The output signal is amplified by $\sim$ 6dB.

5.2 TOAD as an ultra-fast all-optical sampling gate

In order to operate the OCDMA decoder with an equivalent bandwidth of the inverse of chip width, all-optical gating is used to sample the autocorrelation peak that falls within a single chip interval. In our system, we use the terahertz optical asymmetric demultiplexer (TOAD), which is an ultrafast demultiplexer or "AND" gate [19,20], capable of demultiplexing a data pulse that falls within a narrow time gate. Optical time gate widths approaching 1 ps can be achieved. Using enhanced gain recovery techniques, sampling rates for a single TOAD can be as high as 100 GHz [22]. The TOAD requires less than 500 fJ of optical control energy, and can be integrated on a single chip [23].

The Sagnac version of the TOAD is shown in Fig. 8(a). It consists of a 50:50 coupler with its two ports connected together to form a loop. A nonlinear element placed asymmetrically within the loop provides the basis for its switching operation and an intraloop 2×2 coupler is used to inject control pulses into the nonlinear element. The nonlinear element typically used is

a polarization insensitive semiconductor optical amplifier (SOA). When a train of closely spaced data pulses enters the TOAD, each pulse splits into equal clockwise (CW) and counterclockwise (CCW) components which counter-propagate around the loop and arrive at the SOA at slightly different times as determined by the offset, Δx, of the SOA from the midpoint of the loop. The control pulse arrives at the SOA just before the CCW component of the data pulse which is to be demultiplexed, but just after the CW counter-propagating component, inducing nonlinearities in the SOA causing that data pulse components will experience different phase shifts, and consequently recombine and exit the loop at the output port. Here the data pulse gets separated from the control pulse by frequency filtering [28] or other appropriate technique [29]. All other data pulses, for which the counter-propagating components do not straddle the control pulse arrival at the SOA, exit the loop at the input port. As seen in Fig. 8(b), the rising edge of the normalized output intensity, when measured as a function of the delay of the signal pulse relative to the control pulse, is nearly a step function. The duration of the falling edge is limited by the transit time through the SOA, nL/c_0, where n and L are refractive index and length of the SOA respectively, and the duration of the flat top is $2n_g\Delta x/c_0$, where n_g is the refractive index of the loop and c_0 is the speed of light in vacuum. Also, since the TOAD uses an actively biased SOA, it can provide gain to the demultiplexed signal as shown in the inset of Fig. 8(b). The demultiplexed output is larger in amplitude than the input by $\sim$ 6dB. In [21] was demonstrated the elimination of cross correlation signal, MUI (see Fig. 9(b)) using novel TOAD-based OCDMA receiver.

When the receiver was tuned to decode signal from desired transmitter (Tx 3) the cross correlation signal caused by the transmitters Tx 1, Tx 2, and Tx 4 present before the TOAD (see Fig. 9(a)) is clearly eliminated after the TOAD gate (see Fig. 9(b)). Now at the TOAD-based OCDMA receiver output only the autocorrelation/decoded signal from the transmitter Tx 3 is present. Error free operation was observed with BER better than 10^{-9} and no error floor.

To use the TOAD at even higher data rates, several techniques have been demonstrated to reduce the recovery time of the SOA [22]. The switching properties of the TOAD have been also used to design an optical code drop filter for OCDMA ring networks [28].

5.3 Rapidly-reconfigurable optical delay line

As mentioned earlier, the use of tunable optical delay lines at the en/decoders provide capability for dynamic code allocation resulting in more efficient bandwidth utilization. For fast reconfiguration of pulses into different chip positions, tunable delay lines with very low latency are required. We demonstrate the use of a highly scalable parallel delay line [25], which has the potential to tune over a thousand timeslots at 10 Gb/s output bitrate, using 10 GHz electronics, with an average latency less than 40 ns [26]. The schematic of this delay line is shown in Fig. 10. Consider a parallel lattice with M arms and a repetitive modulator gating pattern of period NT (T is the input pulse separation). The delay lattice, with a uniform differential delay $\tau = (N/M) \times T$, temporally compresses the input pulse train by a factor M. By varying the gating pattern to the modulator, the output pulse train can be switched into N different timeslots. For correct operation, the reference pulse (the pulse through the shortest lattice arm) of a timeslot should not coincide with the pulses of other timeslots. This condition gives the constraint that N and M should be co-prime. By using composite values for M, a delay lines with serial-parallel

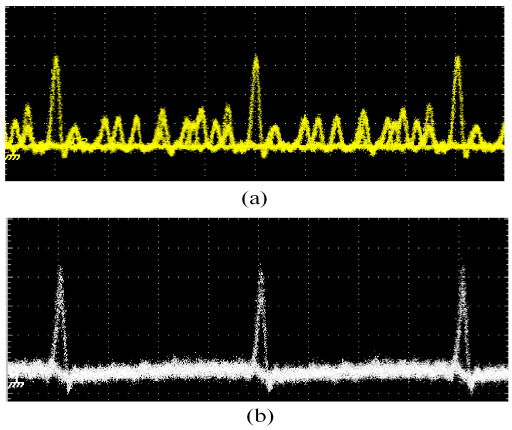

Fig. 9. TOAD-based OCDMA receiver tuned to receive data from desired transmitter: Signal received (a) before the TOAD; (b) after the TOAD -only signal from desired transmitter is present.

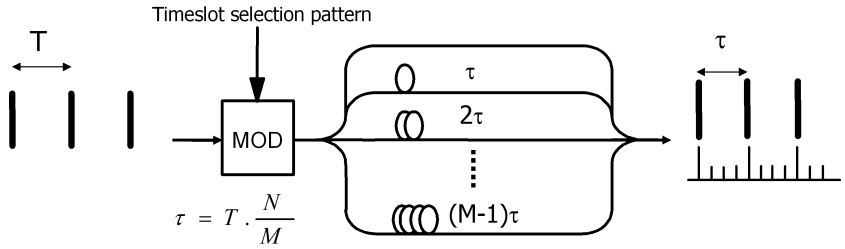

Fig. 10. The schematic of a parallel optical delay line with Ntimeslots and a compression factor of M.

architectures has been demonstrated, which eliminates the need for large parallel lattices for large values of N [26].

Fig. 11 shows the demonstration of a (2, 8) OCDMA encoder with one wavelength (λ_x) passing through the parallel delay line and the other (λ_y) through a fixed time delay. By changing the gating pattern, different codes can be generated as shown in the figure. The gating patterns chosen for the delay line for Fig. 11 are (1000 0000), (0100 0000) and (0000 0010) respectively. The average latency for code transition is 1.2 ns, and the timing accuracy is 1-2 ps. The timing accuracy is determined by the precision of the fiber splicing and can be further improved using various techniques [27].

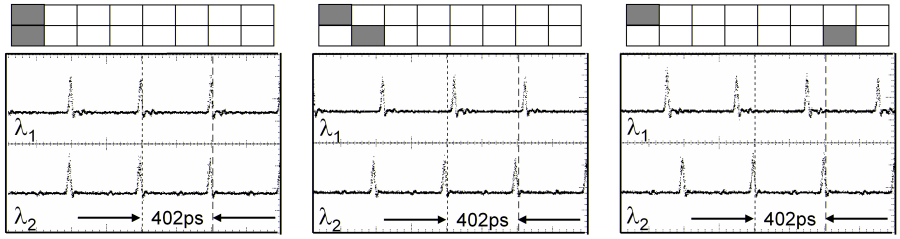

Fig. 11. The operation of a (2,8) OCDMA encoder with λ_1 passing through an 8-timeslot parallel delay line and λ_2 through a fixed time delay. The cartoon shows the matrix representation of the 2D codes generated.

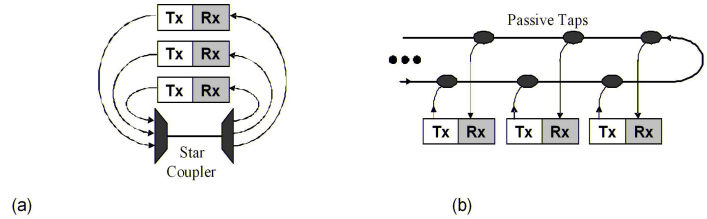

Fig. 12. Two different types of broadcast and select network architectures: (a) star; (b) folded bus.

6 Network Architecture

OCDMA technologies enable many users to simultaneously share optical bandwidth for high speed, bursty networking applications. Architectures for OCDMA naturally lend themselves to broadcast and select structures. The most basic of these, the star network is shown in Fig. 12(a). Transmitted data from N individual users is passively combined using a star coupler and split N ways to broadcast the optical network traffic to all users. The receivers at each node decode the desired data from the network, rejecting the interfering traffic from other users. The star coupler network shown in Fig. 12(a) may be an appropriate architecture for a local area or campus network where all traffic from individual users can be aggregated to a central location. The star architecture can also be used over a longer, point-to-point distance where individual transmitters and receivers are geographically separated. In this architecture, the data from the transmitters at one end are passively combined and transported on the same transmission fiber and then broadcast to all receiving nodes at the destination end. A fiber pair connecting both locations can be used to enable bi-directional traffic flow. Although this provides a means to extend the reach of the network, it assumes that the traffic generated at the transmitters is not destined for receivers adjacent to the transmitter in the local area. This point-to-point network is suitable for applications such as a long-haul OCDMA gateway where a separate network has been used to distribute local OCDMA traffic and only traffic destined for remote nodes is transmitted on the long-haul fiber link.

Figure 12(b) shows the general architecture of a folded optical bus network. Passive optical couplers are used to add OCDMA data from a transmitter to the bus and to tap power from the bus to decode the desired data at the receiver. The folded structure of the bus enables traffic from all transmitters to be aggregated and broadcast on the segment of the bus containing the taps for the receiver. Amplifiers can be inserted on various segments of the network including the folded portion of the bus to compensate for the insertion losses of the taps. Although appropriate for local area OCDMA applications, the folded bus lacks the resiliency needed for highly reliable services. A fiber cut in the bus can bring down the entire network.

OCDMA is ideally suited for broadcast and select network architectures. Depending upon the deployment and applications environment, certain architectures are more suitable than others. By leveraging many of the concepts that have been successfully employed in today's DWDM networks, OCDMA networks will have a more viable path toward practical deployment environments.

7 Conclusion

The advent of high speed optical communications and novel photonic component technologies has enabled the development of broadband optical networks. By using these technologies with novel code designs, OCDMA systems that provide multi-user access to shared optical bandwidth can be realized. We have presented the hardware architecture, node design, and code analysis that support the development of OCDMA systems scalable to 100 potential and more than 10 simultaneous users each operating at 2.5 Gb/s. The chosen carrier-hopping prime codes offer the optimum correlation values, maximum cardinality and measured raw BER $< 10^{-9}$. Novel technologies developed for the system include scalable and rapidly tunable delay lines and ultrafast all-optical TOAD-based OCDMA receiver. We have presented analysis based on our OCDMA system architecture to show the feasibility of error free operation with up to 10 simultaneous users in a broadcast and select star network topology. By demonstrating the feasibility of these novel technologies, viable multi-user OCDMA networks can be realized for broadband fiber communications.

Acknowledgement: This work was supported by the Defense Advanced Research Projects Agency (DARPA) under contract No.: MDA972-03-1-0006.

References

[1] A. Stock, E.H. Sargent: *IEEE Comm. Mag.* **40** (2002) 83-87

[2] J. Shah: *Opt. Phot. News* **14** (2003) 42-47

[3] G.-C. Yang, W.C. Kwong: *Prime Codes with Applications to CDMA Optical and Wireless Networks*, Artech House, Boston MA 2002

[4] F.R.K. Chung, J.A. Salehi, V.K. Wei: *IEEE Trans. Info. Theory* **35** (1989) 595-604

[5] H. Chung, P.V. Kumar: *IEEE Trans. Info. Theory* **36** (1990) 866-873

[6] G.-C. Yang, W.C. Kwong: *IEEE Trans. Comm.* **45** (1997) 1426-1434

[7] L. Tancevski, I. Andonovic: *Elect. Lett.* **30** (1994) 1388-1390

[8] R.M.H. Yim, L.R. Chen, J. Bajcsy: *IEEE Phot. Tech. Lett.* **14** (2002) 714-716

[9] S. Kim, K. Yu, N. Park: *IEEE J. Lightwave Tech.* **18** (2000) 502-511

[10] D.J.G. Mestdagh: *Fundamentals of Multiaccess Optical Fiber Networks, Artech House*, Norwood, MA 1995

[11] W. Huang, M.H.M. Nizam, I. Andonovic, M. Tur: *IEEE J. Lightwave Tech.* **18** (2000) 765-778

[12] E. Inaty, H.M.H. Shalaby, P. Fortier, L.A. Rusch: *IEEE J. Lightwave Tech.* **20** (2002) 166-177

[13] P.R. Prucnal, M.A. Santoro, T.R. Fan: *IEEE J. Lightwave Tech.* **4** (1986) 547-554

[14] J. Chovan, F. Uherek, P. Habovčík: *Laser Physics* **13** (2003) 1112-1118

[15] D.V. Sarwate, in: S.B. Wicker and V.K. Bhargava (Eds.): *Reed-Solomon Codes and Their Applications*, IEEE Press, Piscataway NJ, 1994

[16] I. Vajda, G. Einarsson: *IEEE Trans. Comm.* **35** (1987) 566-568

[17] G.-C. Yang, W.C. Kwong: *Elect. Lett.* **31** (1995) 569-570

[18] K. Mori, H. Takara, S. Kawanashi, M. Saruwatari, T. Morioka: *Elect. Lett.* **33** (1997) 1806-1808

[19] J.P. Sokoloff, P.R. Prucnal, I. Glesk, M. Kane: *IEEE Phot. Tech. Lett.* **5** (1993) 787-790

[20] I. Glesk, J.P. Sokoloff, P.R. Prucnal: *Elect. Lett.* **30** (1994) 339-341

[21] I. Glesk, V. Baby, C.-S. Brès, L. Xu, D. Rand, P. R. Prucnal: *Acta Phys. Slov.* **54** (2004) 245-250

[22] R.J. Manning, D.A.O. Davies, D. Cotter, J.K. Lucek: *Elect. Lett.* **30** (1994) 787-788

[23] I. Glesk, K.I. Kang, P.R. Prucnal: *Opt. Exp.* **1** (1997) 126-133

[24] I. Glesk, K.I. Kang, P.R. Prucnal: *Elect. Lett.* **33** (1997) 794-795

[25] B.C. Wang, I. Glesk, R.J. Runser, P.R. Prucnal: *Opt. Exp.* **8** (2001) 599-604

[26] V. Baby, B.C. Wang, L. Xu, I. Glesk, P.R. Prucnal: *Opt. Comm.* **218** (2003) 235-242

[27] K.I. Kang, K.-L. Deng, S.D. Koehler, I. Glesk, P.R. Prucnal: *Appl. Opt.* **36** (1997) 2533-2536

[28] C.-S. Brès, I. Glesk, P. R Prucnal: *IEEE LEOS* 17^{th} *Annual Meeting*, Puerto Rico, November 2004

[29] D. Senderáková, A. Štrba, J. Chlpík: *Proc. SPIE Vol.* **4016** (2000) 425-429